Influence of Nonlinear Flame Models on Bifurcation Process and Limit Cycles in Gas Turbine Combustors

Giovanni Campa*[1], Sergio Mario Camporeale[1]

[1] Dipartimento di Meccanica, Matematica e Management,
Politecnico di Bari,
via Re David 200, 70125 Bari, Italy
* Corresponding author: g.campa@poliba.it

The aim of this paper is to investigate the influence of the operative parameters characterizing nonlinear flame models. Two shapes of the combustor system are examined: a simple cylindrical configuration and a simple annular one. The heat release fluctuations are coupled to the velocity fluctuations in the burner by means of nonlinear dependence. Two simple polynomial expressions are considered, in which the highest order is the third and the fifth, respectively. Additionally a Flame Describing Approach from the literature is investigated. The bifurcation diagrams for these flame models are obtained, considering the interaction index k as the control parameter. The influence of the time delay on the position of both the Hopf bifurcation point and the fold point is highlighted. The presence of a double mode in the case of annular configuration is also shown.

Introduction

A crucial step in the understanding of the thermoacoustic combustion instabilities is the modeling of the heat release fluctuations. These instabilities are due to coupling between the unsteady heat release rate and the acoustic oscillations inside the combustor. In order to study these instabilities, heat release fluctuations are usually coupled to velocity fluctuations through a linear correlation. Linear flame models are able to predict whether the non-oscillating steady state of a thermoacoustic system is "asymptotically" stable (without oscillations) or unstable (increasing oscillations). However, a thermoacoustic system can reach a permanent oscillating state, known as limit cycle, even when it is linearly stable, if a sufficiently large impulse occurs. A nonlinear analysis is able to predict the existence of this oscillating state and the nature of the bifurcation process.

Culick observed that some stable solid rocket motors would suddenly jump to a self-sustained oscillation state, when pulsed [1]. Since in rocket engines the oscillations have such high amplitudes that the gas dynamics are nonlinear, it was used to consider nonlinear gas dynamics and linear combustion models. This led to demonstrate that nonlinear gas dynamics, even up to third order, is not able to explain triggering [2]. Nonlinear combustion was later taken into account [3–5], assuming that the heat release is a quadratic or rectified (modulus sign) function of the fluctuations of velocity and pressure. It turned out that triggering could be achieved when nonlinear combustion is considered and several typologies of nonlinear flame models were examined.

Similar problems were observed in gas turbine combustion chambers [6–8] and in models of thermoacoustic systems [3, 9, 10]. Lean premixed combustion, which has been introduced in gas turbine engines in order to reduce the emission of NO_x, is often prone to be subjected to ther-

moacoustic instabilities. Since the energy density released in gas turbine combustors is much lower than that in a rocket engine, the thermoacoustic oscillations have amplitude sufficiently low that nonlinear gas dynamics can be neglected. Additionally, in gas turbines the heat release fluctuations are functions of the velocity fluctuations, since the influence of the pressure fluctuations can be neglected [11].

The bifurcation diagram helps in the understanding of the influence of nonlinear combustion, since it shows the amplitude of limit cycles as a function of control parameters. This is useful if there is a known bound on the acceptable oscillation amplitude. It also shows whether the point of linear instability (the so called Hopf bifurcation point) is supercritical or subcritical. This is an important qualitative distinction because: in a subcritical system, high amplitude oscillations occur suddenly when the state becomes linearly unstable and even when the system is linearly stable; in a supercritical system, amplitude oscillations occur only when the system is linearly unstable [12].

In the years several techniques have been proposed in order to track the bifurcation diagrams. One of them is based on obtaining the diagrams by systematic variation of parameters and tracking direct time integration [13, 14]. However this method is computationally expensive.

Another method for obtaining the bifurcation diagrams is numerical continuation [5,15,16]. This approach is based on the iterative solution of a set of parameterized nonlinear equations given an initial guess. The diagram is tracked varying a parameter and including the solutions which satisfy the set of equations for a given state of the system. The unstable limit cycle can also be computed. Compared to other methods, it is very efficient in obtaining the dependence of the solution from the control parameter. However, it takes a long time to map the bifurcation diagram and it can be also too computationally expensive. Thanks to improvements in the method and in the parallel computing, continuation methods are likely to become important tools in nonlinear analysis of thermoacoustics [17].

Juniper [18] and Subramanian [19] used DDE-BIFTOOL, which is a software based on the numerical continuation methods for delay systems [20, 21]. The steady state of the system is evaluated iteratively through the Newton-Raphson scheme and the steady state solution is used for tracking the bifurcation diagram as the control parameter varies.

The use of low-order network models to map the bifurcation diagram as a function of a control parameter has been shown by Campa and Juniper [22], who adopted an approach similar to the Flame Describing Function described by Dowling [23] and Noiray [24, 25]. Hield et al. [26] used an amplitude dependent n-τ model to obtain limit cycles of a ducted V-flame. By means of experimental data, the time delay τ e the interaction index n are written as functions of the amplitude. The use of a framework based on the finite element method (FEM) to study nonlinear flame models was proposed by Pankiewitz and Sattelmayer [27], who examined in the time domain a three-dimensional combustion chamber, predicting the amplitude of limit cycles determined by a nonlinear flame model.

The aim of this paper is to map the bifurcation diagram as a function of a control parameter by using a framework based on the finite element method. The bases of this framework are described in previous works of ours considering linear flame models [28,29]. The approach numerically solves the differential equation problem converted in a complex eigenvalue problem in the frequency domain. The eigenvalue problem is solved by means of a linearization under the hypothesis of small oscillations. From the complex eigenvalues of the system it is possible to ascertain if the corresponding mode is unstable or if the oscillations will decrease in time, i.e. the mode is stable [28].

In the first section of the paper the bases of the nonlinear analysis are explained. In the second section the FEM approach is described, explaining the procedure adopted to track the bifurcation diagrams. In the third section the results are shown, analyzing the bifurcations occurring in a simple Rijke tube for two different nonlinear flame model and examining also the influence of the time delay. The Flame Describing Approach proposed by Dowling [23] is applied to a simple cylindrical duct and the corresponding bifurcation diagram is obtained. The bifurcations from nonlinear flame model characterizing an annular combustion chamber are also investigated in the last part of this paper.

1 Nonlinear Analysis

The mechanisms leading to the onset of combustion instability can be grouped into two categories: linear and nonlinear. A linearly unstable system is the one for which a small perturbation determines the instability. This kind of system is generally not observed in nature [30]. On the other hand, a nonlinearly unstable system can be stable to small perturbations. In this case the system becomes unstable if the initial disturbance is larger than some threshold. This behavior is know as "triggering".

Linear models describing the system behavior are not able to predict triggering instabilities and limit cycle amplitudes. In order to get this kind of information, nonlinearities must be introduced into the model and the analysis. The behavior of a nonlinearly unstable system can change as a control parameter varies. These qualitative changes in the system dynamics are called bifurcations and the parameter values at which they occur is called bifurcation point [12]. Bifurcations are important because provide models of transitions and instabilities as a control parameter is varied.

1.1 Bifurcation Diagrams

Fig. 1 shows two diagrams, describing the bifurcation dynamics as a function of a control parameter R. The variable on the y-axis is the steady state amplitude of the system, which is the limit cycle amplitude. At low values of R the system tends to a zero amplitude stable solution (solid line in Fig. 1). When R reaches the Hopf bifurcation point, the solution of the system becomes unstable. Increasing the value of the control parameter, the solution at zero amplitude remains unstable (dashed line in Fig. 1) and the system starts to oscillate reaching the steady state amplitude (solid line at non-zero amplitudes), known as the limit cycle or the stable periodic solution.

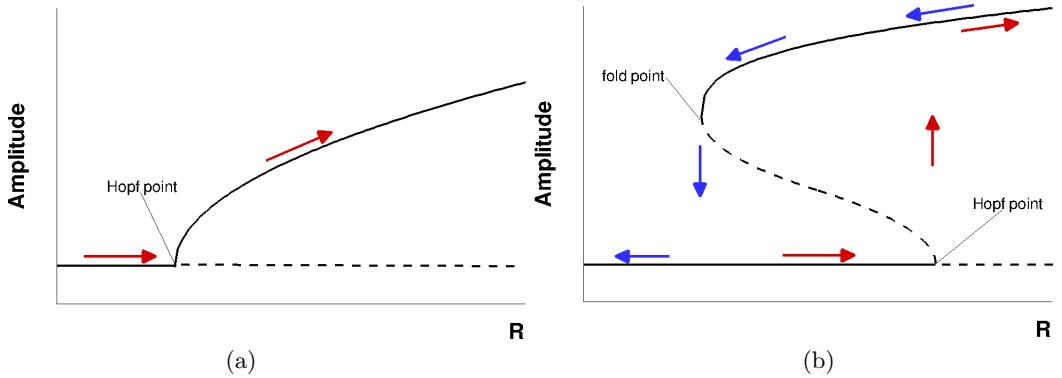

Figure 1: Steady state oscillation amplitude as a function of R for (a) a supercritical bifurcation and (b) a subcritical bifurcation [22]. As the control parameter R is increased, the system follows the red arrow path. As it is decreased, the system follows the blue arrow path.

The nonlinear behavior around the Hopf bifurcation point determines two different types of bifurcation and how the system answers to nonlinear perturbations. The first type is the supercritical bifurcation (Fig. 1a), which is characterized by a gradually increase of the amplitude once reached the Hopf point. In this condition, all perturbations imposed on the system tend to decay to zero only if the Hopf point is not reached, otherwise all the perturbations reach a new stable periodic solution at the limit cycle equilibrium. The second type of behavior is the subcritical bifurcation (Fig. 1b), which is characterized by a sudden increase of the steady state amplitude at the Hopf point. Once reached the limit cycle equilibrium, the perturbations imposed on the system continue to reach a stable periodic solution even for values of R lower than the one corresponding to the Hopf point, until the fold point is reached. For values of R lower than the one corresponding to the fold point, all perturbations decay to zero, as shown by the blue arrow path in Fig. 1b. The dashed line at non-zero amplitudes in Fig. 1b is known as the unstable periodic solution [12]. If the system is triggered to an amplitude below the unstable periodic solution, the imposed perturbations tend

to decay to zero. Otherwise, the imposed perturbations tend to grow reaching the stable periodic solution.

An appropriate analysis for determining the nature of a Hopf bifurcation point is the weakly nonlinear analysis. The weakly nonlinear analysis has been performed on a generic governing equation for fluctuations around the steady state in a single mode thermoacoustic system [17, 22]. Juniper has obtained an expression for the amplitude r of the limit cycle solution

$$r = \pm \left(\frac{4(\zeta - \tau q_1)}{3 q_3 \tau (1 + \tau^2 \omega^2)} \right)^{1/2}, \tag{1}$$

where ζ is the damping coefficient, the heat release q is velocity-coupled with a time delay τ, $q_1 \equiv q'(u(t-\tau)=0)$ (first derivative) and $q_3 \equiv q'''(u(t-\tau)=0)/3!$ (third derivative). Assuming that q_1 is positive, this gives two types of solution, depending on whether q_3 is positive or negative. If q_3 is positive, a subcritical Hopf point is observed, otherwise the Hopf point is supercritical. The same result can be derived with a time-averaging approach. This shows that cubic terms are required in order to predict whether a bifurcation is supercritical or subcritical.

1.2 Nonlinear Flame Model

Nonlinearities are introduced in the flame model. As mentioned in the previous paragraph, heat release fluctuations q' are coupled to the velocity fluctuations u' just upstream the flame zone with a time delay τ. In the linear case and in the time domain it means

$$\frac{q'}{\overline{q}} = -k \frac{u'(t-\tau)}{\overline{u}}, \tag{2}$$

where k is the intensity index, which represents a dimensionless parameter of proportionality between the heat release fluctuations and the velocity fluctuations. The fluctuating variables can be expressed by complex functions of time and position with a sinusoidal form: $q' = \widehat{q}\exp(i\omega t)$ and $u' = \widehat{u}\exp(i\omega t)$. Then the linear flame model in the frequency domain can be written as

$$\frac{\widehat{q}}{\overline{q}} = -k \frac{\widehat{u}}{\overline{u}} \exp(-i\omega\tau). \tag{3}$$

The (linear) flame transfer function used in linear-mode calculations is so defined by:

$$T^L_{flame}(\omega) = \frac{\widehat{q}/\overline{q}}{\widehat{u}/\overline{u}} = -k e^{-i\omega\tau}. \tag{4}$$

In the case a nonlinear flame model is adopted, $\widehat{q}$ has a nonlinear dependence on $\widehat{u}$. The flame transfer function can be obtained following the procedure proposed by Dowling [23] and recalled in [22, 31], so that all the algebraic steps are not shown in this paper. In so doing, the (nonlinear) flame transfer function can be expressed as a multiple of the (linear) flame transfer function and function of frequency and amplitude $r = |\widehat{u}/\overline{u}|$ [31]:

$$T^{NL}_{flame}(\omega, r) = T^L_{flame}(\omega) \cdot NFTF(r) = \widehat{q}^L(\omega) \cdot NFTF(r), \tag{5}$$

where $NFTF$ is the function deriving from the nonlinearity introduced into the flame model [22].

2 Finite Element Method Approach

The nonlinear analysis is carried out by using a finite element method (FEM) based commercial software, COMSOL Multiphysics. This commercial software uses the ARPACK FORTRAN as numerical routine for large-scale eigenvalue problems. It is based on a variant of the Arnoldi algorithm, called the implicit restarted Arnoldi method [32].

Three-dimensional geometries can be examined and complex eigenfrequencies of the system can be detected. This approach numerically solves the differential equation problem converted in a complex eigenvalue problem in the frequency domain and the stability analysis can be conducted.

The fluid is regarded as an ideal gas and flow velocity is considered negligible. The effects of viscosity, thermal diffusivity and heat transfer with walls are neglected, the mean pressure is assumed uniform in the domain. Under such hypotheses, in presence of heat fluctuations, the inhomogeneous wave equation can be obtained [33]

$$\frac{1}{\overline{c}^2}\frac{\partial^2 p'}{\partial t^2} - \overline{\rho}\nabla\cdot\left(\frac{1}{\overline{\rho}}\nabla p'\right) = \frac{\gamma-1}{\overline{c}^2}\frac{\partial q'}{\partial t}, \tag{6}$$

where p' is the pressure fluctuation, γ is the ratio of specific heats, ρ is the density and c is the speed of sound. Under the assumption of zero mean flow velocity, neglecting the effects of the temperature variation, no entropy waves are considered and the pressure fluctuations are related to the velocity fluctuations by

$$\frac{\partial \mathbf{u}'}{\partial t} + \frac{1}{\overline{\rho}}\nabla p' = 0. \tag{7}$$

For the search of the eigenvalues and the eigenmodes of the system, the analysis is performed in the frequency domain and the fluctuating variables are expressed by complex functions of time and position with a sinusoidal form: $p' = \widehat{p}\exp(i\omega t)$, where $\omega = \omega_r + i\omega_i$ is the complex frequency. Its real part ω_r gives the frequency of oscillations, while the imaginary part $-\omega_i$ provides the growth rate at which the amplitude of the oscillations increases per cycle. Then, starting from Eq.(6) the Helmholtz equation in the frequency domain governing the acoustic pressure waves can be written:

$$\frac{\lambda^2}{\overline{c}^2}\widehat{p} - \overline{\rho}\nabla\cdot\left(\frac{1}{\overline{\rho}}\nabla\widehat{p}\right) = -\frac{\gamma-1}{\overline{c}^2}\lambda\widehat{q} \tag{8}$$

where $\lambda = -i\omega$ is the eigenvalue. Combustion is assumed to take place in a single zone, which is acoustically compact in the axial direction and located at the entrance of the combustion chamber. It means the idealistic assumption of a concentrated flame is considered.

2.1 Procedure to Track the Bifurcation Diagrams

The procedure to obtain the bifurcation diagrams using the FEM approach is similar to the one described by Jahnke and Culick [15], which is a continuation method. The general technique is based on fixing all parameters of the system but one and tracing the steady states of the system as a function of this parameter. In this work the control parameter of the bifurcation diagram is the intensity index k, while the only not fixed parameter is the amplitude r. It implies that, each time a value of the amplitude r is assumed to detect the solutions of the eigenvalue problem, a linear flame model is solved. In fact, since the amplitude r is defined as $|\widehat{u}/\overline{u}|$ [31], the $NFTF$ function degenerates to a constant value and the transfer matrix becomes linear. As a consequence, although the flame model is nonlinear, the eigenvalue problem is solved for a linear flame model detecting each point of the bifurcation diagram.

At the beginning, the Hopf bifurcation point is searched for, setting to zero the amplitude r in the nonlinear flame transfer function, so that the flame model becomes linear. Then, the intensity index k is increased until the passage from a stable to an unstable condition is observed, which means when the imaginary part of the complex eigenfrequency becomes negative. The regula falsi method is adopted to detect the point corresponding to zero growth rate, using the last value of k with positive imaginary part and the first value of k with negative imaginary part.

Once the Hopf point, k_H, is identified, the limit cycle solutions are detected. If a supercritical bifurcation is expected, all parameters are fixed but the amplitude r. The search starts from the Hopf point increasing, for each solution point, the intensity index k: the first point is for k slightly greater than k_H with a starting guess for the amplitude r equal to zero or a very low value. The eigenvalue problem is solved for each value of the amplitude r until the change in the sign of the

imaginary part of the complex eigenfrequency is observed: that is from a negative value (unstable condition) to a positive value (stable condition). Again the regula falsi method is used to detect the point corresponding to zero growth rate, so identifying the position of the stable limit cycle solution on the bifurcation diagram. The solution points for the next value of k has the starting guess equal to the previous solution point, and so on. Repeating this procedure for other values of the intensity index k, the bifurcation diagram is obtained.

In the case a subcritical bifurcation is expected, the tracking procedure is the same previously described. Once the Hopf point is identified, the stable limit cycle solution is searched for guessing a starting value of the amplitude r and varying it until the zero growth rate condition is reached for different values of the intensity index k. Differently from the supercritical case, the limit cycle solutions are detected not only for $k > k_H$, but even for $k_F < k < k_H$, where the zero amplitude stable solution and the stable periodic solution coexist. The unstable periodic solution can be tracked starting equally from the fold point or the Hopf point. The points belonging to the unstable periodic solution are characterized by a zero growth rate condition as well and the tracking procedure is again the same of the one for the stable periodic solution.

Connecting the points identified through this procedure, the bifurcation diagrams are obtained.

3 Results

The behavior of various nonlinear flame models is investigated using the FEM approach. Two different configurations are examined: a simple Rijke tube and an annular combustion chamber with multiple burners.

3.1 Simple Rijke Tube

The configuration is a simple Rijke tube with the flame located in a narrow domain at around one quarter of the tube length, which is 3 m. Fig. 2 shows the computational mesh and the location of the heat release is highlighted. The temperature increases from 300 K to 700 K across the combustion zone. The heat release fluctuations q' are coupled to the velocity fluctuations u' with a time delay τ, which is assumed to be constant in the flame domain and its influence on the bifurcation is investigated. Open-end inlet and outlet boundary conditions, $p' = 0$, are considered. The control parameter for mapping the bifurcation diagram is the intensity index k.

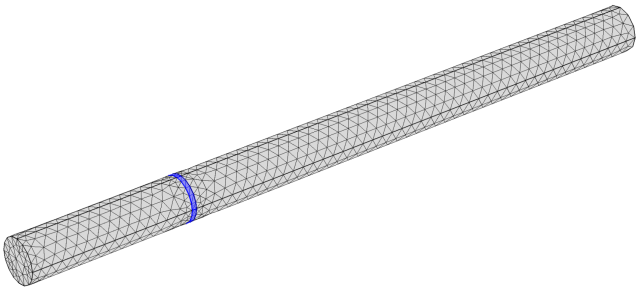

Figure 2: Computational mesh of the simple Rijke tube. The flame location is highlighted in blue.

Two nonlinear flame models are considered. The heat release fluctuations are related to the velocity fluctuations through a polynomial function. Only the influence of the odd-powered polynomial terms are examined because, although even-powered polynomial terms are physically admissible, their contribution to the acoustic energy integrates to zero over a cycle.

For finite disturbances the heat release fluctuation $q'(t)$ is periodic with the same period of the velocity fluctuation $u'(t)$, so that $q'(t)$ can be described by a Fourier series [31]. As in [22,31], only the first harmonic is considered, neglecting higher harmonics, since their influence is small.

3.1.1 First Nonlinear Flame Model

Eq.(9) represents the nonlinear flame model in which the third-powered term is the highest order.

$$\frac{q'(t)}{\overline{q}} = -k\left[\mu_2\left(\frac{u'}{\overline{u}}\right)^3 + \mu_0\frac{u'}{\overline{u}}\right], \tag{9}$$

where μ_2 and μ_0 are coefficient equal to -1 and 0.5, respectively. The function $NFTF$ for this model results to be [22]

$$NFTF = \frac{3}{4}\mu_2 r^2 + \mu_0. \tag{10}$$

The pattern of the nonlinear flame model in Eq.(9) is shown in Fig. 3a, whereas in Fig. 3b the NFTF function of Eq.(10) is shown. The $NFTF$ function is considered only when is positive

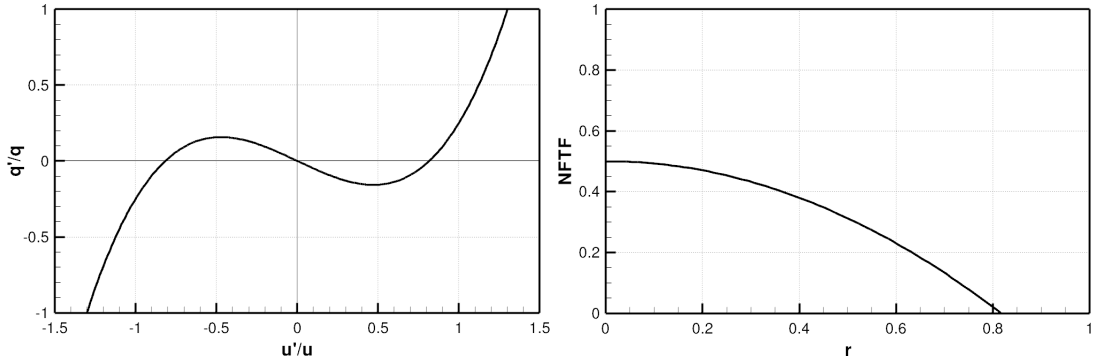

(a) (b)

Figure 3: (a) Flame model and (b) NFTF function for the nonlinear flame model of Eq.(9).

and for positive values of the amplitude r to ensure the physical meaning of the flame model. In this case the $NFTF$ function has a monotone decreasing pattern for increasing amplitudes. The nonlinear flame model in Eq.(9) determines a supercritical Hopf point, as shown in Fig. 4 and as predicted by the weakly nonlinear analysis. In fact, in this case, recalling Eq.(1), the first derivative of heat release expression, q_1, is positive and the third derivative, q_3, is negative, so a supercritical bifurcation is obtained.

The bifurcation diagrams are referred to the first axial mode and tracked for three different values of the time delay τ: 14, 15 and 20 ms, as shown in Fig. 4. The influence of the time delay is on the position of the Hopf point, as shown in Fig. 4. In fact for $\tau = 14\ ms$ the Hopf point occurs for $k = 0.11$, for $\tau = 15\ ms$ the Hopf point occurs for $k = 0.95$ and for $\tau = 20\ ms$ the Hopf point occurs for $k = 0.73$. The amplitude of the stable limit cycle solution tends to be the same for all the cases at higher values of k. The eigenfrequency of the mode is 72.0 Hz and it changes if the system is linearly stable, whereas it remains constant at non-zero amplitudes. Tab.(1) shows the values of the frequencies in the Hopf point for the three values of τ.

Table 1: Frequencies in the Hopf point for the nonlinear flame model of Eq.(9) for different values of τ.

Modal Frequency	$\tau = 14\ ms$ f_H	$\tau = 15\ ms$ f_H	$\tau = 20\ ms$ f_H
72.0 Hz	71.4 Hz	66.7 Hz	75.0 Hz

Additionally, there are values of the time delay for which the system is stable or unstable at any value of the intensity index k, so that no bifurcation diagram can be tracked. In order to have a

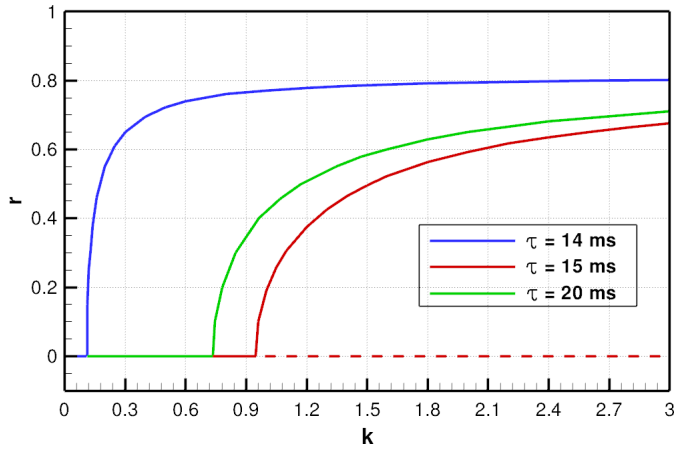

Figure 4: Bifurcation diagram for three different value of the time delay for the nonlinear flame model of Eq.(9).

better comprehension of the influence of the time delay, growth rate is plot against the frequency for different values of τ, as in Fig. 5, where the patterns are tracked assuming a constant value of the amplitude, $r = 0.4$, and for three values of the intensity index k: $0.2, 0.5, 0.8$. The time delay τ is varied from 5 to 25 ms and each curve has a quasi-circular pattern. Fig. 5 shows that, increasing

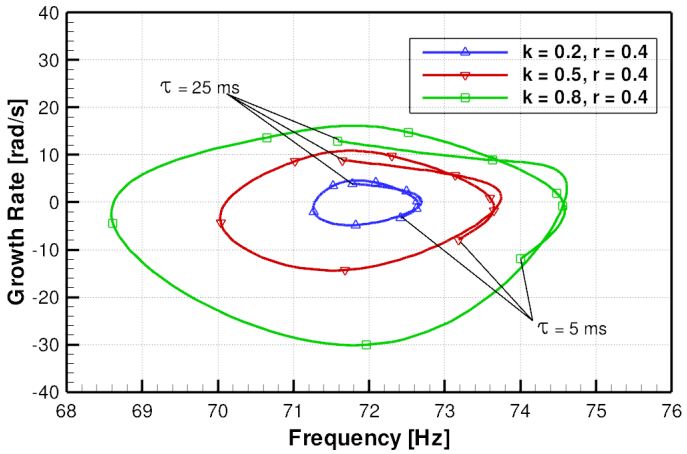

Figure 5: Frequency and growth rate of the first eigenmode of a Rijke tube for the nonlinear flame model of Eq.(9).

the intensity index, frequency and growth rate again decrease or increase depending on the value of the time delay: frequency tends to depart from the modal frequency; the growth rate tends to increase its absolute value, reaching more unstable conditions if it is positive and more stable conditions if it is negative. It is due to the increase of the intensity of the heat release, leading to conditions more prone to become unstable.

3.1.2 Second Nonlinear Flame Model

Eq.(11) represents the nonlinear flame model in which the fifth-powered term is the highest order:

$$\frac{q'(t)}{\overline{q}} = -k\left[\mu_4\left(\frac{u'}{\overline{u}}\right)^5 + \mu_2\left(\frac{u'}{\overline{u}}\right)^3 + \mu_0\frac{u'}{\overline{u}}\right], \tag{11}$$

where μ_4, μ_2 and μ_0 are coefficient equal to -1, 1 and 0.2, respectively. The function $NFTF$ for this model results to be

$$NFTF = \frac{5}{8}\mu_4 r^4 + \frac{3}{4}\mu_2 r^2 + \mu_0. \tag{12}$$

The pattern of the nonlinear flame model in Eq.(11) is shown in Fig. 6a, whereas in Fig. 6b the $NFTF$ function of Eq.(12) is shown. Even in this case the $NFTF$ function is considered only

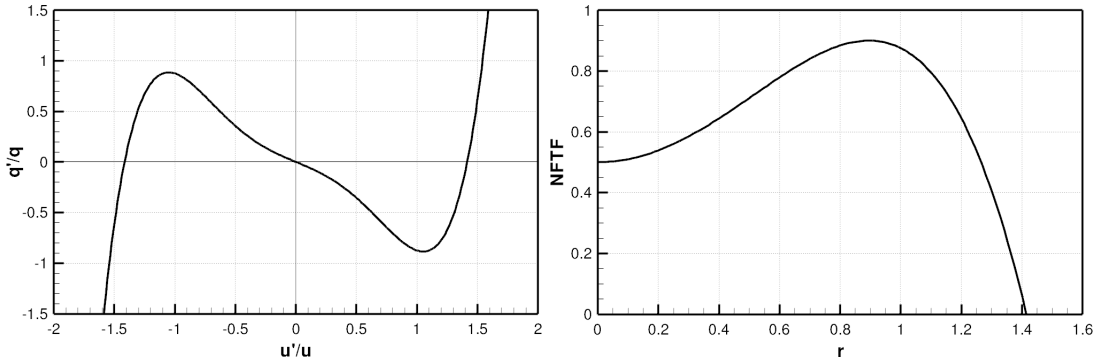

(a) (b)

Figure 6: (a) Flame model and (b) NFTF function for the nonlinear flame model of Eq.(6).

when is positive and for positive values of the amplitude r to ensure the physical meaning of the flame model. In this case the $NFTF$ function has an initial increase reaching its maximum value, after which it decreases until zero is reached. The bifurcation diagram for this case is shown in Fig. 7, referred to the first axial mode of the Rijke tube. The influence of the time delay τ on the bifurcation diagrams is also investigated, considering three different values of τ: 14, 15 and 20 ms, as shown in Fig. 7. The influence of τ is again on the position of the Hopf point and the fold point.

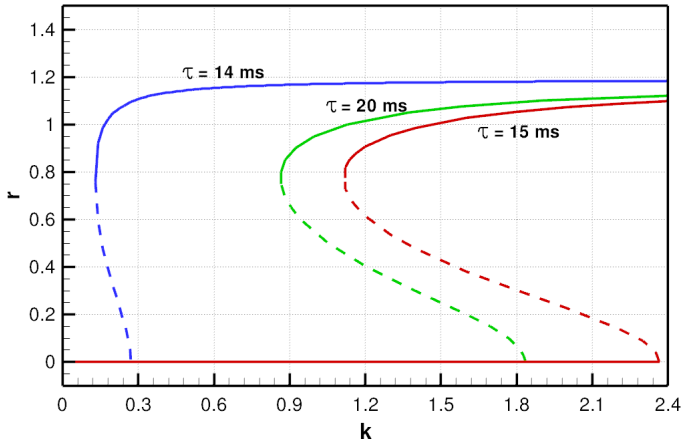

Figure 7: Bifurcation diagram for three different value of the time delay for the nonlinear flame model of Eq.(11).

For $\tau = 14$ ms the Hopf point occurs for $k = 0.27$ and the fold point for $k = 0.13$, for $\tau = 15$ ms the Hopf point occurs for $k = 2.37$ and the fold point for $k = 1.12$, for $\tau = 20$ ms the Hopf point occurs for $k = 1.83$ and the fold point for $k = 0.87$. The amplitude of the stable limit cycle solution tends to be the same for all the cases at higher values of k. The eigenfrequency of the mode is 72.0 Hz and it changes if the system is linearly stable (decreasing for $\tau = 14$ ms and for $\tau = 15$ ms, increasing for $\tau = 20$ ms), whereas it remains constant at non-zero amplitudes. These three values of τ are the same examined for the nonlinear flame model of Eq.(9) and the values of

the frequencies in the Hopf point are the same of the ones shown in Tab.(1). As a consequence, for a certain value of the time delay, the mode tends to reach the same frequency in the Hopf point, and keeping it constant at non-zero amplitudes, independently of the nonlinear flame model.

Additionally, even in this case there are values of the time delay for which the system is stable or unstable at any value of the intensity index k, so that no bifurcation diagram can be tracked. An analysis of the influence of the time delay on frequency and growth rate for certain values of k and r can be performed, obtaining results similar to the ones shown in Fig. 5.

3.1.3 Describing Function Analysis

In this section the describing function analysis by Dowling [23] is used. It is based on information coming from the Bloxsidge et al. experiment [34,35]: ethylene is burned in a circular duct in which the flame is stabilized in the wake of an axisymmetric centre-body [34]. The examined geometry is similar to that shown in Fig. 2, but the dimensions are different: the length of the section upstream the flame zone is 1.17 m, the length of the section downstream the flame zone is 0.73 m [23,35]. The temperature increases from 300 K to 700 K across the flame zone. Closed-end inlet and open-end outlet boundary conditions are considered. The expression of the nonlinear flame model is [23]

$$\frac{\widehat{q}}{\overline{q}} = \frac{\widehat{u}}{\overline{u}} a(r,\omega) F(\omega) \exp(-i\omega\tau). \tag{13}$$

$a(r,\omega)$ is a normalized complex gain, which can be assimilated to the NFTF described in this paper. Dowling [23] considers $F(\omega) = f(\Omega)$, where Ω is a non-dimensional frequency. The configuration examined in this paper is characterized by a constant cross section area, so that the non-dimensional frequency Ω is null and the corresponding function f has gain equal to 1 and null phase, as shown in Fig.2 in [23]. As highlighted by Dowling, the complex gain $a(r,\omega)$ is quite always real and it has a weak dependence on frequency. Its magnitude is shown in Fig. 8, considering $\Omega = 0$.

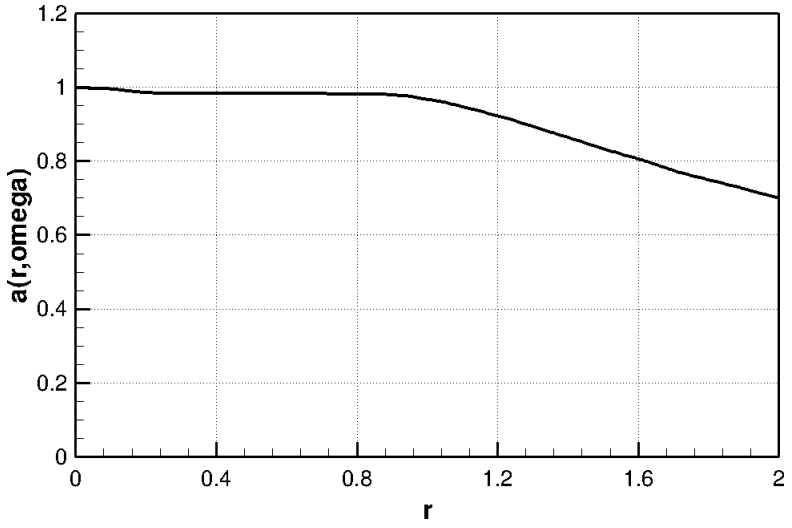

Figure 8: Normalized complex gain $a(r,\omega)$, Eq.(13).

The bifurcation diagram for the nonlinear flame model of Eq.(13) is obtained varying the interaction index k. A supecritical bifurcation is obtained, Fig. 9. After the appearence of the Hopf bifurcation point ($k \sim 1.24$), there is a sudden increase of the bifurcation curve up to $a \sim 0.9$. It is consistent with the shape of $a(r,\omega)$, which is nearly equal to 1 for a large range of values of the amplitude r, Fig. 8. It means that the flame model is quasi-linear for small values of the amplitude. Since the bifurcation point is supercritical, there is not an hysteretic behavior, but

there is a narrow range of values of k with a critical behavior. In fact, when the interaction index is around 1.25 and the amplitude of the oscillations lower than 1, a small perturbation can bring the system in either the stable zone or the unstable zone. If the system is in the stable zone, the oscillations decay to zero. If the system is in the unstable zone, the oscillations grow up to the stable limit cycle solution. The straight line after the Hopf bifurcation point corresponds to the

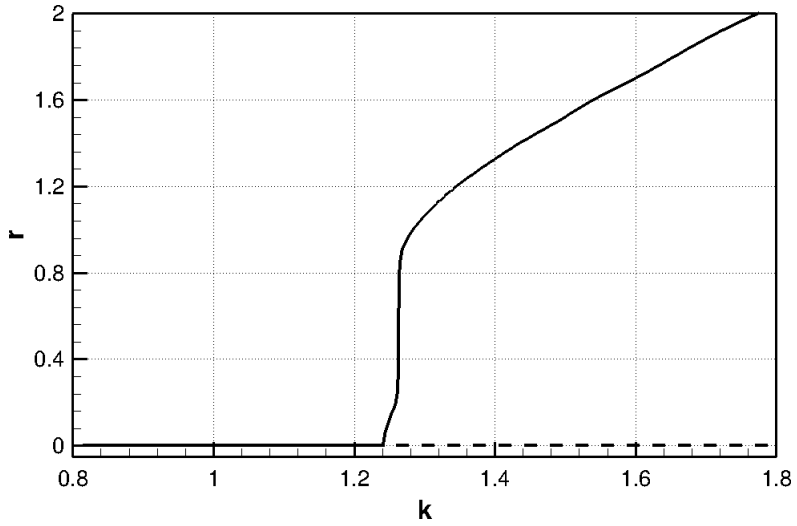

Figure 9: Bifurcation diagram for the describing function analysis proposed by Dowling [23].

quasi-linear behavior of the flame model, since there is a clear separation between the stable and the unstable zones.

3.2 Annular Combustion Chamber

The examined configuration is characterized by an annular plenum and an annular combustion chamber connected by a ring of twelve straight ducts (representing the burners). The geometrical configuration is similar to the one introduced by Pankiewitz and Sattelmayer [27]. The mean diameter is 0.437 m, the external diameter of the plenum is 0.540 m and of the combustion chamber is 0.480 m. The length of the plenum is 0.200 m and of the combustion chamber is 0.300 m. Each burner has a diameter of 0.026 m and a length of 0.030 m. Temperature in the combustion chamber is 2.89 times the temperature on the plenum. Flame is assumed to be concentrated in a narrow zone at the entrance of the combustion chamber, as shown in Fig. 10, and it is composed of twelve equal parts, one corresponding to each burner. In so doing the heat release fluctuations are coupled to the velocity fluctuations of the corresponding burner, following the ISAAC (Independence Sector Assumption in Annular Combustors) assumption, introduced by Sensiau et al. [36]. This assumption states that *the heat release fluctuations in a given sector [of the combustion chamber] are only driven by the fluctuating mass flow rates due to the velocity perturbations through its own swirler*. Closed-end inlet and outlet are assumed as boundary conditions ($u' = 0$). Mean flow is neglected also in this case. Tab.2 shows the first four modes of the system without heat release fluctuations. Eigenmodes are denoted with the nomenclature (l, m, n), where l, m and n are, respectively, the orders of the pure axial, circumferential and radial modes.

3.2.1 Polynomial Nonlinear Flame Model

The nonlinear flame model of Eq.(11), in which the fifth-powered term is the highest order, is introduced for heat release fluctuations, assuming $\mu_4 = -1$, $\mu_2 = 1$ and $\mu_0 = 0.2$ (in Fig. 6 the flame model and the $NFTF$ function). Again the heat release fluctuations q' are coupled to the velocity fluctuations u' with a time delay τ. which is assumed to be constant.

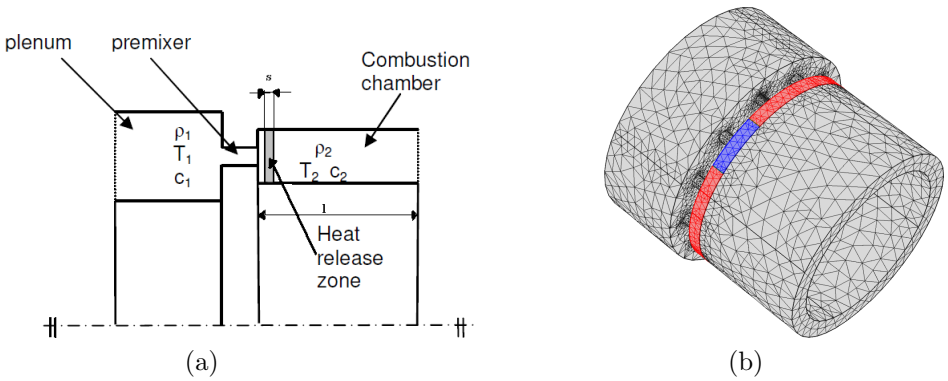

Figure 10: (a) Sketch of the annular combustion chamber. (b) Computational grid and flame zone highlighted in red. One of the twelve sectors, in which the flame zone is divided, is highlighted in blue.

Table 2: Frequencies of the first four modes of the annular combustion chamber.

Mode Shape	(1,0,0)	(0,1,0)	(1,1,0)	(0,2,0)
Frequency [Hz]	309.0	445.2	733.3	837.0

Fig. 11 shows the bifurcation diagrams for the first azimuthal mode, whose modeshape is located in the combustion chamber (the modal frequency is 733.3 Hz, Tab.(2)). It is observed that for time delay τ equal to 10 and 14 ms, the first azimuthal mode occurs at two different frequencies, so that there are two bifurcation diagrams for each value of τ. Tab.(3) shows the frequencies at which the first azimuthal mode occurs in the Hopf point for three different values of τ: e.g., for $\tau = 10$ ms the first azimuthal mode appears both at 700 Hz and at 750 Hz. Only for $\tau = 2$ ms the mode appears at one frequency. Further investigation has shown that this mode splitting appears when the time delay exceeds a certain value.

The bifurcation diagrams for $\tau = 2$ ms, one of the two at 10 ms and one of the two at 14 ms coincide. This behavior can also be observed in Tab.(3), since the frequency at which the limit cycle solution appears (750 Hz) is the same for the three cases. For this mode the time period is around 1.33 ms, so that the chosen values of the time delay are multiple of it. The amplitude of the limit cycle solution is the same independently of the time delay and so of the location of the Hopf point. Similarly, the fold point occurs at the same amplitude. The modeshapes of the two azimuthal modes appearing at two different frequencies are nearly the same. There is a perfect coincidence of the modeshapes at zero amplitude and at limit cycle condition. A similar condition can be observed for the axial mode [37].

Table 3: Frequencies in the Hopf point for the nonlinear flame model of Eq.(11) for different values of τ for the first azimuthal mode in the combustion chamber of the annular combustion chamber in Fig. 10.

Modal Frequency	$\tau = 2$ ms f_H	$\tau = 10$ ms f_H	$\tau = 14$ ms f_H
733.3 Hz	750.0 Hz	700.0 Hz 750.0 Hz	714.3 Hz 750.0 Hz

A further investigation is carried out considering the condition in which the time delay τ is

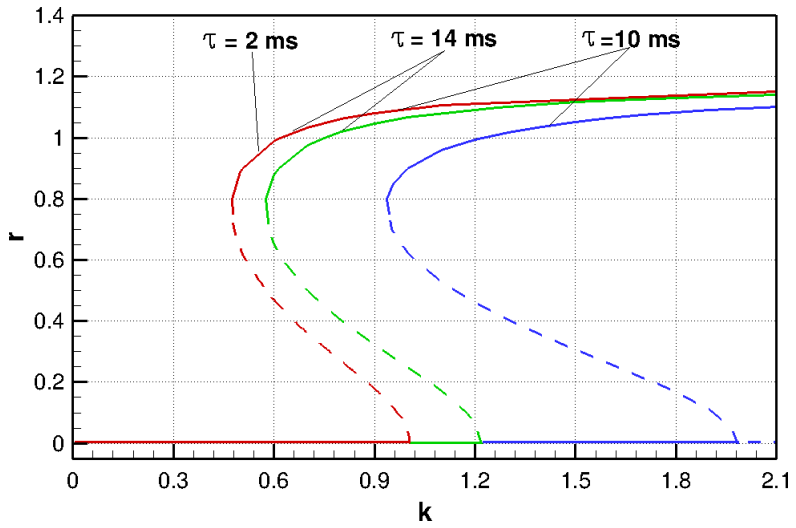

Figure 11: Bifurcation diagram for three different value of the time delay for the nonlinear flame model of Eq.(11) for the first azimuthal mode in the combustion chamber of the annular combustion chamber in Fig. 10.

equal to 10 ms. The corresponding bifurcation diagrams are isolated in Fig. 12: the blue track corresponds to the 700 Hz bifurcation, while the red track corresponds to the 750 Hz bifurcation. The arrows in the figure represent the growth rate of the mode in such condition: a positive growth rate means an increase in the amplitude of the oscillations and hence an up-facing arrow, a negative growth rate means a decrease in the amplitude of the oscillations and hence a down-facing arrow. If the system is triggered to an amplitude below the unstable periodic solution of the mode at 750 Hz, the imposed perturbations tend to decay to zero. If the interaction index k is included in the range between the two fold points, if the triggering amplitude is in this range, the imposed perturbations start to grow until the amplitude of the corresponding limit cycle amplitude of the mode at 750 Hz is reached. If the system is triggered to an amplitude below the unstable periodic solution of the mode at 700 Hz, the imposed perturbations decay to zero. If the triggering amplitude is included in the bifurcation diagram of the mode at 700 Hz, the imposed perturbations grow until the limit cycle amplitude of the mode at 700 Hz is reached. If the system is triggered to an amplitude between the two stable periodic solutions, the system can either reach one limit cycle or the other.

In order to highlight such a behavior, the growth rate of the two modes at different amplitudes in the case of $k = 1.2$ and $\tau = 10$ ms is shown in Fig. 13. The mode at 700 Hz is characterized by lower values of the growth rate, so that the system is attracted by the stable solution at this mode [12]. This behavior can be observed for quite all the values of the interaction index k, as shown in Fig. 14. The two plotted surfaces represent the growth rate field at different values of the interaction index and the amplitude. The upper surface (the green one) corresponds to the mode at 750 Hz, whereas the lower surface (the blue one) corresponds to the mode at 700 Hz. It can be seen that their intersection with the surface at zero growth rate (the red one) identify the periodic solution on the bifurcation diagram. The stable periodic solution is the intersection edge when, increasing the amplitude, the system moves from positive to negative growth rate. The unstable periodic solution is the intersection edge when, decreasing the amplitude, the system moves from negative to positive growth rate.

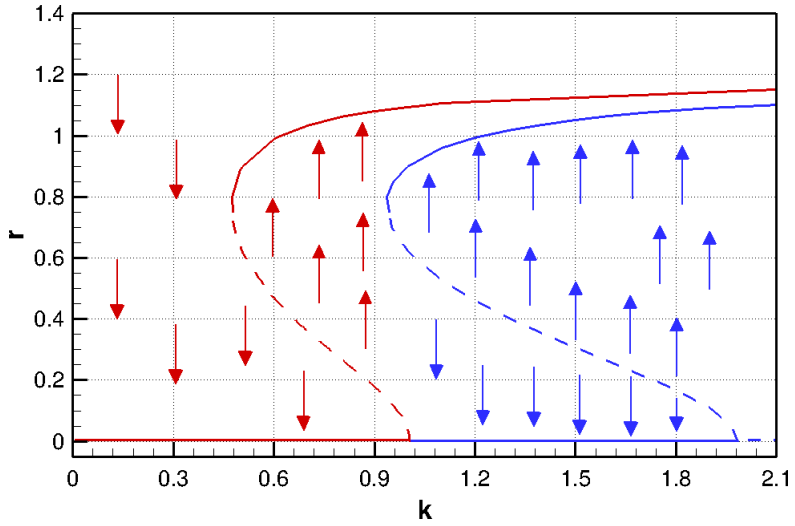

Figure 12: Bifurcation diagram for the nonlinear flame model of Eq.(11) for the first azimuthal mode in the combustion chamber of the annular combustion chamber in Fig. 10 when $\tau = 10\ ms$.

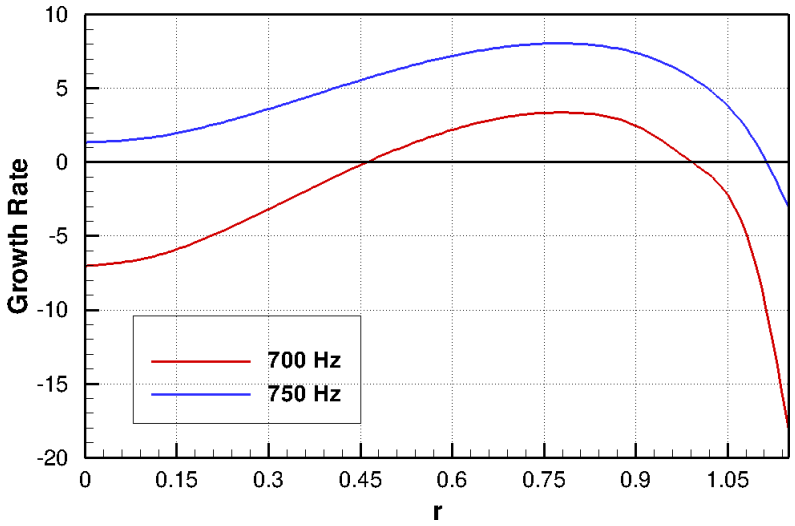

Figure 13: Growth rate of the mode at several values of the amplitude in the condition of $\tau = 10\ ms$ and $k = 1.2$.

Conclusion

The nonlinear behavior of the system is considered within the flame model. Heat release fluctuations are coupled to the velocity fluctuations through a nonlinear polynomial correlation. The behaviour of the system is determined by the nature of the Hopf bifurcation. A framework based on the finite element method in the frequency domain is used to track the bifurcation diagrams. Simple Rijke tube configuration and a simple annular combustion chamber are examined.

The kind of bifurcation depends on the nonlinear flame model, independently of the geometrical configuration examined, following the predictions of the weakly nonlinear analysis. The influence of the time delay on the bifurcations is investigated. The main points are:

1. the influence of the time delay is only on the position of Hopf point and fold point;

2. the amplitude of the limit cycle solution and the amplitude of the oscillations at the fold

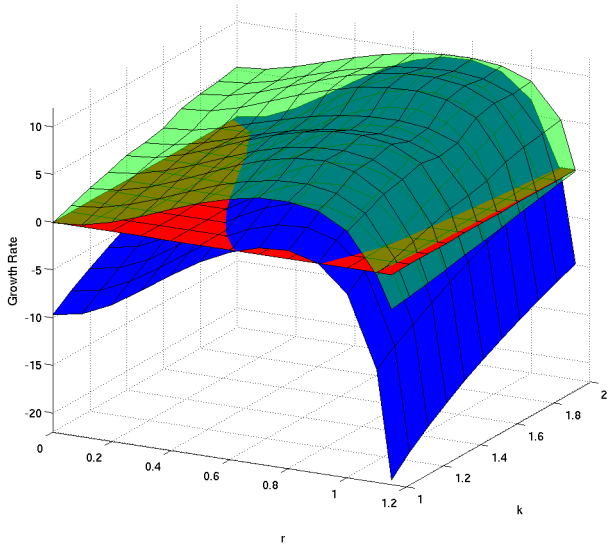

Figure 14: Growth rate of the mode at several values of the amplitude and of the interaction index in the condition of $\tau = 10\ ms$.

point are not influenced by variations of the time delay;

3. the frequency of the mode changes only in linear conditions, whereas remains constant when the limit cycle solution is reached;

4. for a Rijke tube configuration the frequency of the first axial mode for a certain value of τ reaches the same value at the Hopf point independently of the nonlinear flame model;

5. for a simple annular configuration a mode can occur at two different frequencies, so that two bifurcation diagrams for one mode can be tracked. The system is more prone to reach the condition with the lower growth rate.

Finally, the Flame Describing Approach proposed by Dowling [23] is introduced in the flame model and the corresponding bifurcation diagram is obtained. The bifurcation is supercritical and the limit cycle solution is characterized by a straight line after the Hopf point and for small amplitudes of the oscillations: it is due to the quasi-linear behavior of the flame model at small amplitudes.

References

[1] F.E.C. Culick. *Unsteady Motions in Combustion Chambers for Propulsion Systems*. AGARD, AG-AVT-039, 2006.

[2] V. Yang, S.I. Kim, and F.E.C. Culick. Triggering of longitudinal pressure oscillations in combustion chambers. 1: Nonlinear gas dynamics. *Combustion Science and Technology*, 72(4):183–214, 1990.

[3] J. Wicker, W. Greene, S.I. Kim, and V. Yang. Triggering in longitudinal combustion instabilities in rocket motors: Nonlinear combustion response. *Journal of Propulsion and Power*, 12(6):1148–1158, 1996.

[4] J.D. Baum, J.N. Levine, and R.L. Lovine. Pulsed instability in rocket motors: A comparison between predictions and experiment. *Journal of Propulsion and Power*, 4(4):308, 1988.

[5] N. Ananthkrishnan, S. Deo, and F.E.C. Culick. Reduced-order modeling and dynamics of nonlinear acoustic waves in a combustion chamber. *Combustion Science and Technology*, 177:1–27, 2005.

[6] T. Lieuwen. Experimental investigation of limit cycle oscillations in an unstable gas turbine combustor. *Journal of Propulsion and Power*, 18(1):61–67, 2002.

[7] J. Lepers, W. Krebs, B. Prade, P. Flohr, G. Pollarolo, and A. Ferrante. Investigation of thermoacoustic stability limits of an annular gas turbine combustor test-rig with and without helmholtz resonators. *ASME paper, GT2005-68246*, 2005.

[8] T. Lieuwen and V. Yang. *Combustion Instabilities in Gas Turbine Engines*. AIAA, 2005.

[9] K. Balasubramanian and R.I. Sujith. Thermoacoustic instability in a rijke tube: Nonnormality and nonlinearity. *Physics of Fluids*, 20:044103, 2008.

[10] K. Balasubramanian and R.I. Sujith. Nonnormality and nonlinearity in combustion-acoustic interaction in diffusion flames. *Journal of Fluid Mechanics*, 594:29–57, 2008.

[11] W. Polifke. Combustion instabilities. *von Kármán Institute Lecture Series, March 2004*.

[12] S.H. Strogatz. *Nonlinear Dynamics and Chaos*. Westview Press, 2001.

[13] J.P. Moeck, M.R. Bothien, S. Schimek, A. Lacarelle, and C.O. Paschereit. Subcritical thermoacoustic instabilities in a premixed combustor. *14th AIAA/CEAS Aeroacoustics Conference, 2946*, 2008.

[14] S. Mariappan and R.I. Sujith. Modeling nonlinear thermoacoustic instability in an electrically heated rijke tube. *48th AIAA Aerospace Sciences Meeting Including the New Horizons Forum and Aerospace Exposition, 2010-25*, 2010.

[15] C.C. Jahnke and F.E.C. Culick. Application of dynamical systems theory to nonlinear combustion instabilities. *Journal of Propulsion and Power*, 10:508–517, 1994.

[16] V.S. Burnley. *Nonlinear Combustion Instabilities and Stochastic Sources*. PhD Dissertation, California Inst. of Technology, Pasadena, USA, 1996.

[17] M.P. Juniper. Triggering in thermoacoustics. *AIAA Aerospace Sciences Meeting, 9-12 January 2012, Nashville, Tennessee*, 2012.

[18] M.P. Juniper. Triggering in the horizontal rijke tube: Non-normality, transient growth and bypass transition. *Journal of Fluid Mechanics*, 667:272–308, 2011.

[19] P. Subramanian, S. Mariappan, R.I. Sujith, and P. Wahi. Bifurcation analysis of thermoacoustic instability in a horizontal rijke tube. *Int. Journal of Spray and Combustion Dynamics*, 2(4):325–356, 2010.

[20] K. Engelborghs and D. Roose. Numerical computation of stability and detection of hopf bifurcations of steady state solutions of delay differential equations. *Advances in Computational Mathematics*, 10:271–289, 2010.

[21] K. Engelborghs, T. Luzyanina, and D. Roose. Numerical bifurcation analysis of delay differential equations using dde-biftool. *ACM Transactions on Mathematical Software*, 28:1–21, 2002.

[22] G. Campa and M. Juniper. Obtaining bifurcation diagrams with a thermoacoustic network model. *ASME paper, GT2012-68241*, 2012.

[23] A.P. Dowling. A kinematic model of a ducted flame. *Journal of Fluid Mechanics*, 394:51–72, 1999.

[24] N. Noiray, D. Durox, T. Schuller, and S. Candel. A unified framework for nonlinear combustion instability analysis based on the flame describing function. *Journal of Fluid Mechanics*, 615:139–167, 2008.

[25] N. Noiray, D. Durox, T. Schuller, and S. Candel. A method for estimating the noise level of unstable combustion based on the flame describing function. *International Journal of Aeroacoustics*, 8:157–176, 2009.

[26] P. Hield, M. Brear, and S. Jin. Thermoacoustic limit cycles in a premixed laboratory combustor with open and choked exits. *Combustion and Flame*, 156:1683–1697, 2009.

[27] C. Pankiewitz and T. Sattelmayer. Time domain simulation of combustion instabilities in annular combustors. *Journal of Engineering for Gas Turbine and Power*, 125(2):677–685, 2003.

[28] S.M. Camporeale, B. Fortunato, and G. Campa. A finite element method for three-dimensional analysis of thermoacoustic combustion instability. *Journal of Engineering for Gas Turbine and Power*, 133(1):011506, 2011.

[29] G. Campa, S.M. Camporeale, E. Cosatto, and G. Mori. Thermoacoustic analysis of combustion instability through a distributed flame response function. *ASME paper, GT2012-68243*, 2012.

[30] T. Lieuwen. *Investigation of Combustion Instability Mechanisms in Premixed Gas Turbines*. PhD Dissertation, Georgia Institute of Technology, Atlanta, USA, 1999.

[31] S.R. Stow and A.P. Dowling. A time-domain network model for nonlinear termoacoustic oscillations. *ASME paper, GT2008-50770*, 2008.

[32] R. Lehoucq and D. Sorensen. Arpack: Solution of large scale eigenvalue problems with implicity restarted arnoldi methods. www.caam.rice.edu/software/arpack. User's Guide.

[33] A.P. Dowling and S.R. Stow. Acoustic analysis of gas turbine combustors. *Journal of Propulsion and Power*, 19(5):751–765, 2003.

[34] G.J. Bloxsidge, A.P. Dowling, and P.J. Langhorne. Reheat buzz: an acoustically coupled combustion instability. part 2. theory. *Journal of Fluid Mechanics*, 193:445–473, 1988.

[35] P.J. Langhorne. Reheat buzz: an acoustically coupled combustion instability. part 1. experiment. *Journal of Fluid Mechanics*, 193:417–443, 1988.

[36] C. Sensiau, F. Nicoud, and T. Poinsot. Thermoacoustic analysis of an helicopter combustion chamber. *AIAA paper, AIAA-2008-2947*, 2008.

[37] G. Campa, M. Cinquepalmi, and S.M. Camporeale. Influence of nonlinear flame models on sustained thermoacoustic oscillations in gas turbine combustion chambers. *ASME paper, GT2013-94495*, 2013.